Supplemental material

Bean et al., https://doi.org/10.1083/jcb.201804111

Table S1 is a separate Excel file showing Ypt35 and Spo71 FIMO hits.

Table S2 is a separate Excel file showing strains (A), plasmids (B), and primers (C) used in this study.

Reference

Biegert, A., and J. Söding. 2008. De novo identification of highly diverged protein repeats by probabilistic consistency. *Bioinformatics.* 24:807–814. https://doi.org/10.1093/bioinformatics/btn039

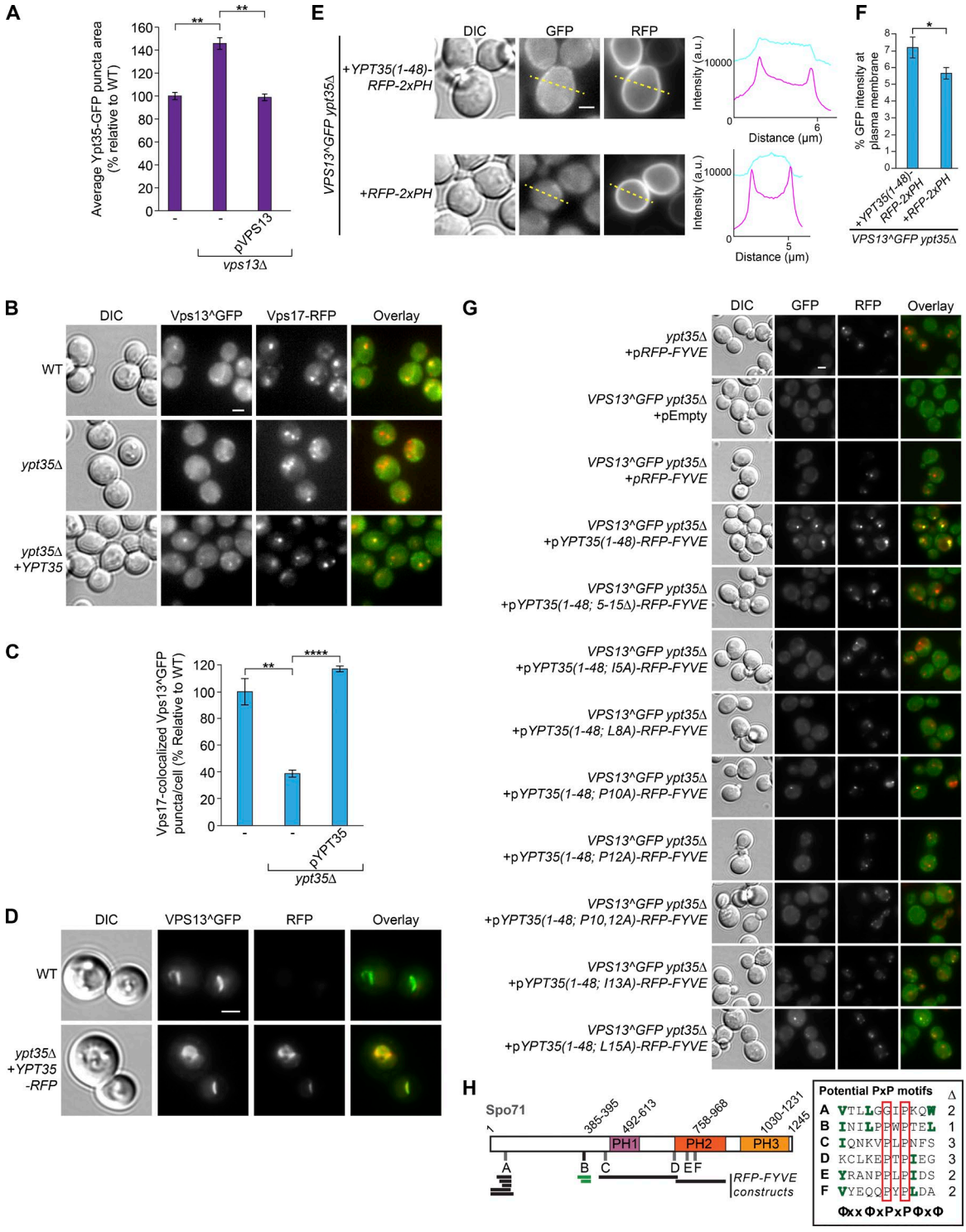

Figure S1. **Additional measures of Vps13 and Ypt35 localization. (A)** Loss of *VPS13* causes an increase in the area of Ypt35 puncta. Two-tailed equal variance *t* test; *n* = 3, cells/strain/replicate ≥1,047; **, P < 0.01. **(B)** Vps13^GFP is dependent on Ypt35 for localization to Vps17-RFP labeled endosomes. **(C)** Quantitation of Vps13^GFP puncta that colocalize with Vps17-RFP. Two-tailed equal variance *t* test; *n* = 3, cells/strain/replicate ≥1,910; **, P < 0.01; ****, P < 0.0001. **(D)** Vps13^GFP colocalizes with Ypt35-RFP at NVJs. **(E)** Ypt35(1–48)-RFP-2×$PH_{PLC\delta}$ recruits Vps13^GFP to the plasma membrane. Line scans indicate the intensity of GFP (cyan) and RFP (magenta) signals along the dashed line. **(F)** Quantitation of Vps13^GFP recruitment to the plasma membrane, measured as the percent of the total cell intensity colocalizing with the RFP construct at the plasma membrane. Two-tailed paired *t* test; *n* = 4, ≥1,775 cells/strain/replicate; *, P < 0.05. **(G)** All Ypt35(1–48)-RFP-FYVE constructs were expressed and localized to the vacuolar rim/puncta, and in cases where Vps13^GFP was recruited to puncta, the tagged proteins colocalized. DIC, differential interference contrast. **(H)** A schematic of Spo71 showing the locations of potential PxP Vps13-interaction motifs with partial matches to the consensus ϕxx ϕxPxPϕxϕ, where ϕ is a hydrophobic residue. The number of deviations from the consensus for each potential motif is indicated under Δ. Regions chosen for RFP-FYVE constructs are indicated by bars below; constructs indicated by green or black bars respectively did or did not promote formation of colocalizing Vps13^GFP puncta. Bars, 2 µm. Error bars indicate SEM.

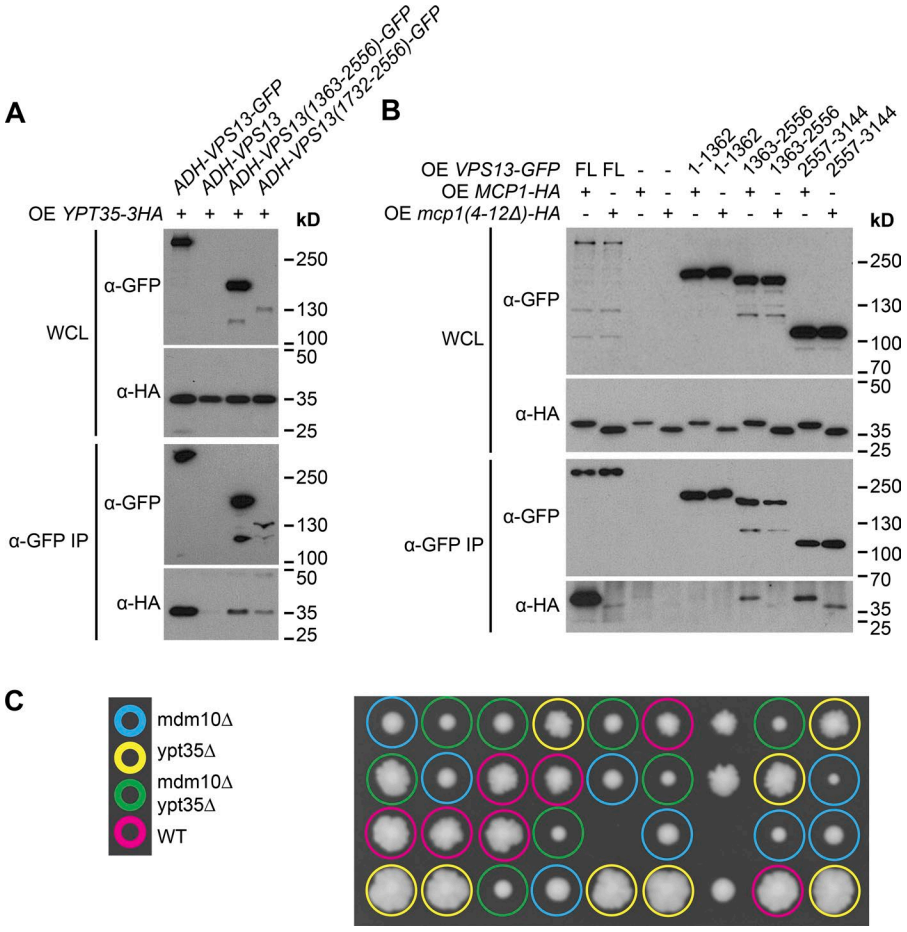

Figure S2. **Additional assessments of Vps13 adaptor interactions. (A)** Ypt35-3HA binds the minimal DUF1162-containing Vps13(1,732–2,556)-GFP fragment. *ADH1pr*-driven WT or truncated Vps13-GFP was immunopurified, and coprecipitating *ADH1pr*-expressed Ypt35-3HA was detected by immunoblot. **(B)** Mcp1-3HA interacts with DUF1162–containing Vps13 fragments but not a C-terminal fragment in a PxP motif–dependent manner. *ADH1pr*-driven Vps13-GFP was immunopurified, and coprecipitating WT or mutant *ADH1pr*-overexpressed Mcp1-3HA was detected. IP, immunoprecipitation; WCL, whole-cell lysate. **(C)** Tetrad dissections of an *mdm10Δ* × *ypt35Δ* cross show the *mdm10Δ* and *ypt35Δ* mutations do not exhibit synthetic lethality.

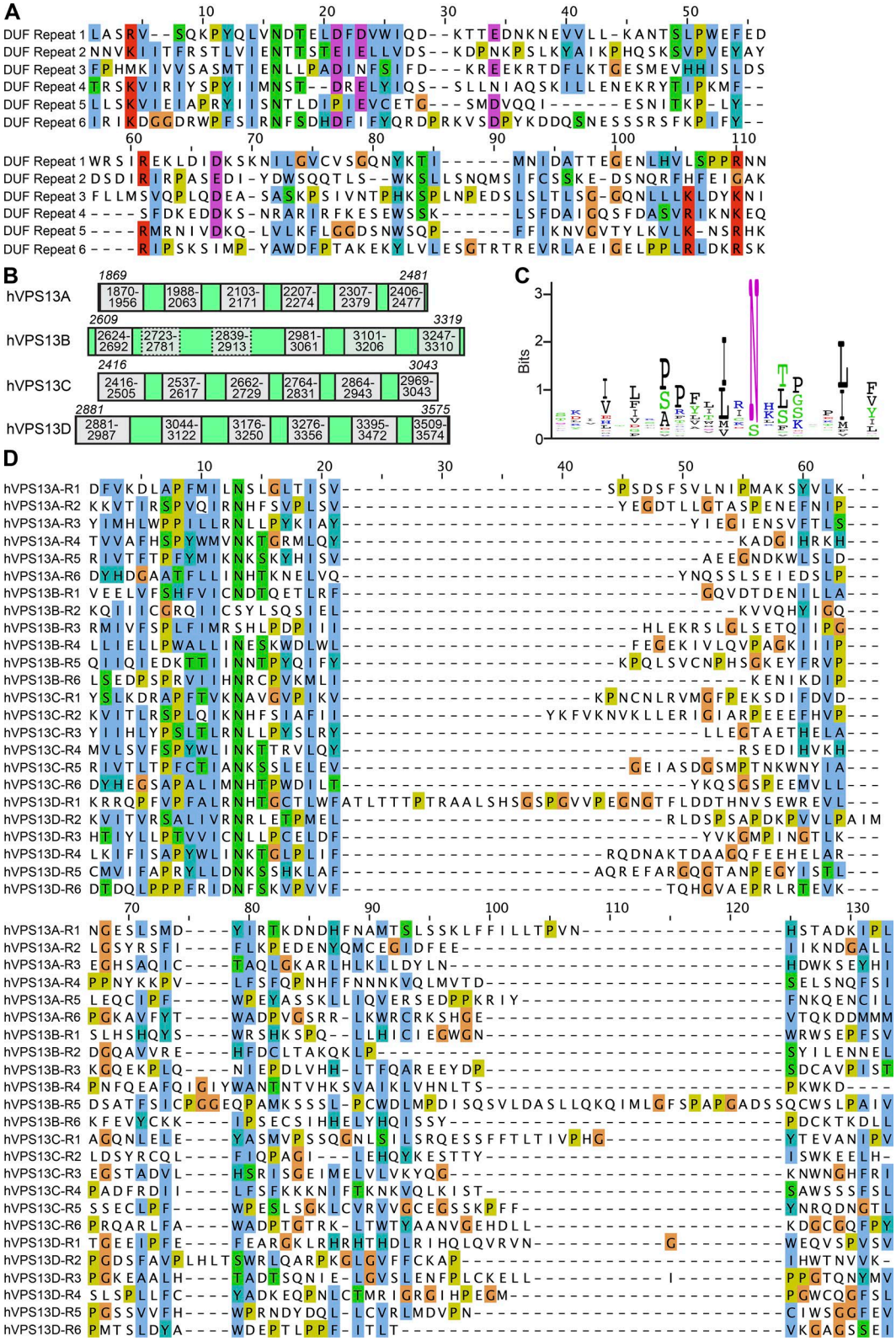

Figure S3. **Complete alignments of Vps13 DUF1162 repeats. (A)** Alignment of the six *S. cerevisiae* DUF1162 repeats identified by HHrepID (Biegert and Söding, 2008). **(B)** DUF1162 repeats identified by HHrepID in the four *Homo sapiens* VPS13 proteins. Dotted boxes indicate repeats lacking an otherwise invariant asparagine residue. **(C)** WebLogo of the conserved N-terminal region of all 24 human DUF1162 repeats. **(D)** Alignment of the 24 *H. sapiens* DUF1162 repeats in VPS13A/B/C/D.